IJST, Transactions of Mechanical Engineering, Vol. 38, No. M1, pp 79-90
Printed in The Islamic Republic of Iran, 2014

EXPERIMENTAL ANALYSIS OF UN-UNIFORM FIN WIDTH HEAT SINKS WITH BASE PLATE*

R. MOHAN

Dept. of Mechanical Engineering, Sona College of Technology, India
Email: rmohan12@ gmail.com

Abstract– The thermal performances of the heat sink with un-uniform fin width designs with base plates and carbon nano tube coating were investigated experimentally and numerically. Realistic, manufacturable geometries are considered for minimizing thermal resistance at low velocity. The parameters include the Reynolds number (Re = 5000 - 25000), five fin width design (Type - a to Type - e), three base plates (copper, ccc and copper-diamond composite) and carbon nano tube coating. In this study, the effects of base plates and nano coating on thermal performance of heat sinks with un-uniform fin width are experimentally studied. Experimental results show that among the many design parameters such as base plates and nano coating, composite base plate has a more significant influence on the thermal performance of heat sinks. It is also found that there is potential for optimizing the un-uniform fin width heat sinks with base plates and nano coating.

Keywords– Base plates and nano coating, forced cooling of electronic devices, computational fluid dynamics, un-uniform fin width heat sinks

1. INTRODUCTION

With the rapid development of electronic technology, electronic appliances and devices are now a part of our daily life. The heat flux per unit area has increased significantly over the past few years due to the condition of multifunction, shrinking package size, high clock speed, and higher power dissipations. Among the novel methods for thermal management of the high heat fluxes found in microelectronic devices, forced air cooled heat sinks are the most effective at heat removal, especially for desktop computer. Thus the thermal and flow characteristics of heat sinks have been the interest of many investigators. A large number of recent investigations have studied the forced air cooled heat sinks for electronics cooling as well as to compare the flow and heat transfer characteristics of heat sinks. The thermal performance of the heat pipe and heat sink for electronics cooling under different conditions has been studied by many researchers. Also, the literature on the variety of heat sinks used in different electronic applications has been identified. Finned heat sinks are most widely used as a thermal solution to ensure the reliability of electronic devices [1, 2]. There are many researches on heat transfer in electronic cooling, such as heat pipe [3-4], jet impingement cooling [5-6] and microchannel heat sink [7], etc. Several researchers have examined the thermal and flow characteristics of various heat sinks extensively. Seyf and Layeghi [8] have carried out a numerical analysis to determine flow and heat transfer characteristics of elliptical pin fin heat sinks with and without metal foam inserts. Kuznetsov et al. [9] investigated numerically the thermal characteristics of a pin-fin heat sink. An aluminum foam heat sink placed horizontally in a channel was modeled as a hydraulically and thermal anisotropic porous medium. It was shown that the anisotropy in the permeability and the effective thermal conductivity changes the

*Received by the editors March 18, 2013; Accepted September 28, 2013.

heat transfer rate of the heat sink substantially, and the optimum porosity for maximum thermal dissipation depends significantly on the pin-fin thickness, the pin-fin height and the Reynolds number. Sivasankaran et al. [10] have studied the experimental investigation of parallel plate fin and cross cut pin fin heat sinks where the heating element is placed asymmetrically. The thermal performance, heat transfer coefficient and efficiencies have been compared for various heat sinks. Kim et al. [11] have compared the thermal performances of the two types of heat sinks most commonly used in the electronic equipment cooling: plate-fin and pin-fin heat sinks. In order to obtain the fluid flow and thermal characteristics of heat sinks, an experimental investigation is conducted. Jonsson, and Moshfegh [12] have conducted tests in a wind tunnel with seven types of heat sinks including plate fin, strip fin, and pin fin heat sinks. In the case of strip fin, and pin fin heat sinks, both in-line and staggered arrays have been studied. Kim et al. [13] have conducted the thermal optimization of a plate-fin heat sink with the fin thickness varying in the direction normal to the fluid flow. Kim and Kim [14] have experimentally studied the effects of cross-cuts on the thermal performance of heat sinks under the parallel flow condition. Hwang and Lui [15, 16] studied the heat transfer and pressure drop characteristics between pin-fin trapezoidal ducts with straight and lateral outlet flows. The effect of pin arrangement for the ducts of different direction outlet flow was also examined. Moreover, a similarity of the pin Reynolds number dependence of row-averaged Nusselt number was developed. An experimental study was conducted to investigate the heat transfer from a parallel flat plate heat sink under a turbulent air jet impingement by Sansoucy et al. [17]. The forced convection heat transfer rates from a flat plate and from a flat plated heat sink under an impinging confined jet have been obtained. In addition, the experimental results were compared with the numerical predictions obtained in an earlier study. They concluded that the numerical analysis in a previous study was adequate for appraising the mean heat transfer rate in jet impingement for situations of thermal management of electronics. Chiang and Chang [18] and Chiang et al. [19] developed the response surface methodology (RSM) and applied grey-fuzzy logic to find the optimal values of designing parameters of a pin fin type heat sink under constraints of mass and space limitations to achieve the high thermal performance. The optimal designing parameters have been carried out and verified by conducting confirmation experiments. Li et al. [20] and Li and Chen [21] investigated the thermal performance of pin-fin and plate-fin heat sinks with confined impingement cooling by using infrared thermography. The results show that the thermal resistance of the heat sinks decreases with the increased Reynolds number of the impinging jet. However, the reduction of the thermal resistance decreases gradually as the Reynolds number increases. Moreover, it revealed that the influence of fin width is more obvious than the fin height. In addition, the optimal impinging distance increases with the increasing Reynolds number. Finally, they concluded that the thermal performance of the pin-fin heat sinks is superior to that of the plate-fin heat ones. Furthermore, the thermal performance of pin-fin heat sinks with air impingement cooling was performed numerically and experimentally by Li and Chen [22]. Ozturk [23] has investigated the forced cooling of heat sinks mounted on CPUs. Thermal parameters such as heat sink effectiveness, turbulence models, radiation and geometry of heat sinks have been analyzed using commercial CFD programs Fluent and Icepak. Later, some improvements on heat sinks were decided after carrying out several simulations and the results were found to be in good agreement with the experimental values. Ozturk and Tari [24] have investigated the flow and temperature fields inside the chassis and also the three different commercial heat sink designs have been analysed by using CFD. The flow obstructions in the chassis and the resulting air circulation that affect the heat sink temperature distribution are studied. It is recommended that a maximum temperature distribution in the heat sink can be reduced by changing the geometry, base thickness and especially, replacing aluminum with copper as the heat sink material. The four copper fins are used at the center of the heat sink for reducing hot spots. Mohan and Govindarajan [25-26] have studied the performance of slot parallel plate fin heat sink, double base plate heat sink,

elliptical fin heat sink and pin fin heat sink with various base plate materials. The experimental results are compared with CFD results. In this work, the fin thickness, the fin pitch, and the fin height has been optimized. Yoshida and Morigami [27] made a new material composed of diamond and copper and studied its thermal properties. The effects of diamond particle sizes and the volume fractions of diamond on both thermal conductivity and the coefficient of thermal expansion (CTE) were investigated. Atashafrooz and Gandjalikhan Nassab [28] studied the simulation for incompressible laminar mixed convection flow of a radiating gas in a vertical duct by using CFD techniques. Earlier research on the performance analysis of the heat sink with the effect of various parameters has been carried out. However, less work has been done on the effect of different base plate materials, thickness and nano coating. The purpose of this study is to examine the effect of the fin shape on the thermal performance of the heat sink with base plate and nano coating. In this paper, the experimental analysis of heat sinks with base plate and nano coating in thermal-fluid characteristics will be investigated and compared numerically.

2. EXPERIMENTAL SETUP AND PROCEDURE

A schematic diagram of the experimental setup is shown in Fig. 1. The width and height of the wind tunnel duct are 150 mm and 120 mm, respectively and the wind tunnel duct has acrylic plates of a thickness of 10 mm. A thin film heater fabricated using Kapton-coated stainless steel of a thickness of 0.3 μm is attached to the bottom surface of a heat sink. It plays the role of a heat source as it is connected to a DC power supply. To reduce heat loss, a Bakelite plate with 12 mm thickness is attached to the bottom surface of the thin film heater. The Bakelite plate is then attached to the bottom of the wind tunnel duct using four screws. There is no clearance between the wind tunnel duct and the two sides of the heat sink. The heat sink base and base plate is flush with the bottom wall of the wind tunnel duct. There are 12 pressure taps at the top wall of the wind tunnel duct to measure the pressure drop across the heat sink along the air flow direction. The spacing between any two adjacent pressure taps is 10 mm. The first pressure tap is located 30 mm upstream of the heat sink and the last one is located 30 mm downstream of the heat sink. The pressure drop across the heat sink is the difference between the pressures measured at the first and the last pressure taps. Seventeen K-type thermocouples were used for temperature measurement. To measure the maximum temperature of the heat sink, eight thermocouples were mounted through 5 mm deep holes at the base plate of the heat sink, which are positioned along the centerline of the heat sink. They are 6 mm apart. The first thermocouple is positioned 6 mm from the leading edge of the heat sink and the last one is positioned 6 mm from the end of the heat sink. One thermocouple was used to measure the inlet temperature. To measure the heat loss another eight thermocouples were attached to the Bakelite plate and the inner surface and outer surface of the wind tunnel duct. The uncertainty of each thermocouple is approximately 0.75%. A HP 34970A data acquisition unit is utilized to convert the electrical signals measured by the thermocouples into temperature information. The test procedures were as follows: the desired volume flow rate of the air was generated by a suction-type blower. The heater was then powered up to a heat load of 20W and was allowed to stabilize. The heat load was calculated by multiplying the current and the voltage drop through the heater. The measured heat losses in the experiments were in the range of 3–7% of the heat load supplied by the heater. Once the heat load was fixed, the base temperature of the heat sink was monitored. A steady-state was assumed when the change in the maximum temperature of the heat sink was smaller than ±0.1°C for a period of 5 min. The maximum base temperature of the heat sink and the bulk mean inlet temperature were used to calculate the thermal resistance of the heat sink.

$$R=\frac{T_{w,max}-T_{bm,in}}{Q}$$

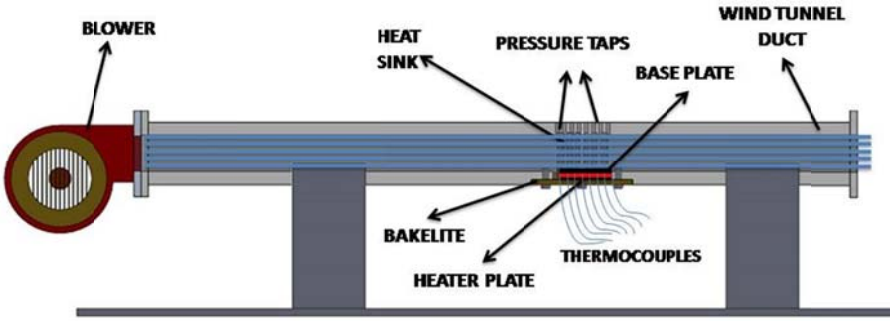

Fig. 1. A Schematic diagram of the experimental setup

a) Verification

To check the validity of the present study, the experimental results of the thermal resistance of a heat sink of uniform width of the fins under the conditions Re = 5000 to 25000 and Q = 20 W , one of the experimental cases, were compared with the available numerical results of the literature [21]. Figure 2 shows that the experimental results of the thermal resistance of a heat sink are in good agreement with numerical results proposed by Yang and Peng [21] within 5.6%. Based on these comparisons, it is clear that the experiments in this study were properly conducted. Moreover, a total number of cells, 69347, 97086 and 135920 were employed to assess the grid independence as shown in Fig. 3. The deviations of the thermal resistance predicted using meshes with 69347 and 97086 cells are 4.5% and 1.5% from that obtained using a mesh with 135920 cells. The results of the grid sensitivity study showed that the simulations based on the 97086 meshes provide satisfactory numerical accuracy. The average error between simulation results and experimental results is about 8%.

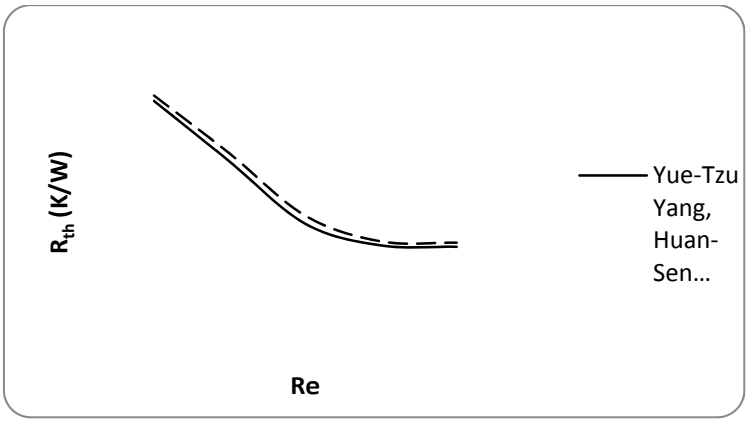

Fig. 2. Verification of experimental value

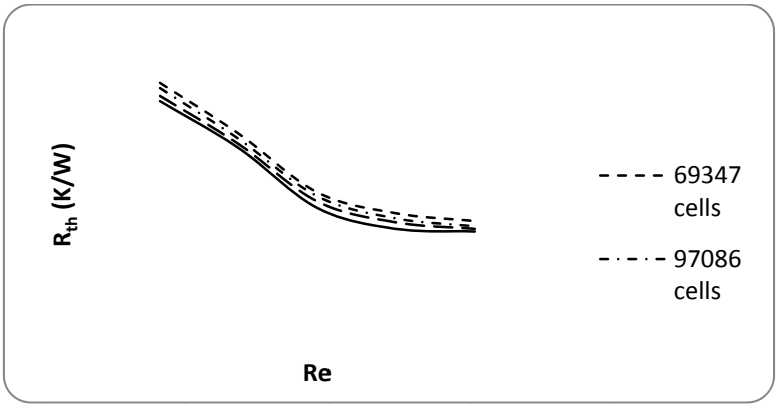

Fig. 3. Grid independent test

3. GOVERNING EQUATIONS FOR FLUID FLOW AND HEAT TRANSFER

The forced convective fluid flow is governed by the continuity equation, momentum equations (Navier-Strokes equations) and energy equation. The incompressible, turbulent, and steady state fluid flow is considered. The buoyancy and radiation heat transfer effects are neglected. In addition, the thermo physical properties of the fluid are assumed to be constant. The three-dimensional governing equations of mass, momentum, turbulent kinetic energy, turbulent energy dissipation rate, and energy in the steady turbulent main flow using the standard k - ε model are as follows:

Continuity Equation

$$\nabla\left(\rho\,\vec{V}\right) = 0 \tag{1}$$

Momentum Equations

$$\nabla\left(\rho u\vec{V}\right) = -\frac{\partial p}{\partial x} + \frac{\partial \tau_{xx}}{\partial x} + \frac{\partial \tau_{yx}}{\partial y} + \frac{\partial \tau_{zx}}{\partial z} + B_x \tag{2}$$

$$\nabla\left(\rho v\vec{V}\right) = -\frac{\partial p}{\partial y} + \frac{\partial \tau_{xy}}{\partial x} + \frac{\partial \tau_{yy}}{\partial y} + \frac{\partial \tau_{zy}}{\partial z} + B_y \tag{3}$$

$$\nabla\left(\rho w\vec{V}\right) = -\frac{\partial p}{\partial z} + \frac{\partial \tau_{xz}}{\partial x} + \frac{\partial \tau_{yz}}{\partial y} + \frac{\partial \tau_{zz}}{\partial z} + B_z \tag{4}$$

Energy Equation

$$\nabla\left(\rho h\vec{V}\right) = -p\nabla\vec{V} + \nabla(k\,\nabla T) + \dot{g} \tag{5}$$

Turbulent kinetic energy k Equation

$$\overline{U}\frac{\partial k}{\partial x} + \overline{V}\frac{\partial k}{\partial y} + \overline{W}\frac{\partial k}{\partial z} = \frac{\partial}{\partial x}\left(\nu + \frac{\nu_t}{\sigma_k}\frac{\partial k}{\partial x}\right) + \frac{\partial}{\partial y}\left(\nu + \frac{\nu_t}{\sigma_k}\frac{\partial k}{\partial y}\right) + \frac{\partial}{\partial z}\left(\nu + \frac{\nu_t}{\sigma_k}\frac{\partial k}{\partial z}\right) + P_k - \varepsilon \tag{6}$$

Turbulent energy dissipation rate ε Equation

$$\overline{U}\frac{\partial \varepsilon}{\partial x} + \overline{V}\frac{\partial \varepsilon}{\partial y} + \overline{W}\frac{\partial \varepsilon}{\partial z} = \frac{\partial}{\partial x}\left(\nu + \frac{\nu_t}{\sigma_\varepsilon}\frac{\partial \varepsilon}{\partial x}\right) + \frac{\partial}{\partial y}\left(\nu + \frac{\nu_t}{\sigma_\varepsilon}\frac{\partial \varepsilon}{\partial y}\right) + \frac{\partial}{\partial z}\left(\nu + \frac{\nu_t}{\sigma_\varepsilon}\frac{\partial \varepsilon}{\partial z}\right) + C_{\varepsilon 1}\frac{\varepsilon}{k}P_k - C_{\varepsilon 2}\frac{\varepsilon^2}{k} \tag{7}$$

P_k is the production of the turbulent kinetic energy that is usually modeled as

$$P_k = \nu_t\, S^2$$

Where S is the modulus of the mean strain rate tensor. The turbulent viscosity is given by

$$\nu_t = C_\mu\,\frac{k^2}{\varepsilon}$$

This model contains five constants and the most commonly used values for those are

$$C_\mu = 0.09\,,\ C_{\varepsilon 1} = 1.14\,,\ C_{\varepsilon 2} = 1.92,\ \sigma_k = 1.0,\ \sigma_\varepsilon = 1.3$$

a) Computational domain and boundary conditions

The computational domain consists of heat sinks defined as solid and surrounding fluid and is shown in Fig. 4. It has a height of H, flow length L, and width W_c. The heat sink is placed 0.3 m from the inlet of the domain. The working fluid is air and flows through the enclosure. The top, bottom and side walls are adiabatic. Three dimensional steady state flow is presented and the fluid is incompressible and all materials are isotropic. In order to investigate the physical characteristics of the heat transfer, a combination of inlet, outlet, and wall boundary conditions is applied in computational domain. Since Navier-Stokes equations are solved inside the domain, the boundary conditions for velocity and temperature fields are needed.

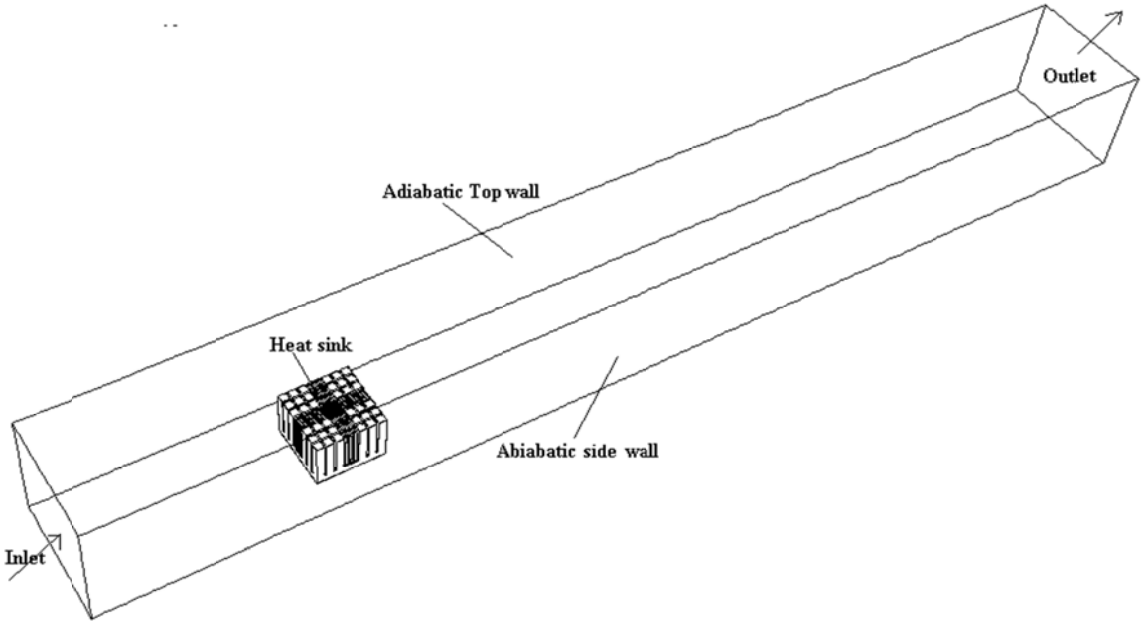

Fig. 4. Computational domain of the un-uniform fin width heat sink

b) Hydrodynamics and thermal boundary conditions

The velocity is zero at all boundaries except the inlet and outlet. The chip is represented as a 30mm by 30mm square area at the bottom of the heat sink. A uniform heat flux is given over the chip area which is calculated based on the total heat dissipation value of 20W.

1. At the inner walls in the domain no-slip boundary condition is applied.

   $u = 0, v = 0, w = 0.$

2. At inlet

   $p = p_{in}, T = T_{in}, u = u_{in}, v = 0, w = 0.$

2. At outlet

   $p = p_{out}, \frac{dT}{dz} = 0, u = 0, v = 0.$

c) Solution procedure

The governing equations for the fluid and solid regions are solved using FLUENT 6.3 which uses a finite volume method. In this study, the segregated solver is used as the solution algorithm which solves the governing equations of mass, momentum and energy sequentially. A first order upwind scheme is

employed for the discretization of the all the variables and the SIMPLE scheme has been used for the pressure-velocity coupling. The numerical solution is considered to be converged when residual is 10^{-4} for the continuity and momentum equations and 10^{-8} for the energy equation. In the present study, the RNG k-ε model is used as turbulence model. Radiation heat transfer helps the heat sink cool by 0.2 to 0.5 K. Therefore, it is concluded that the radiation can be ignored.

4. RESULTS AND DISCUSSION

In this study, the dimensions of the aluminum heat sinks with different un-uniform fin width designs are depicted in Fig. 5. The effects of the different base plates, Reynolds number and the fin dimensions on the thermal performance are investigated. The parameters considered in this study include five Reynolds numbers (Re = 5000–25000), three base plates (copper, ccc and copper-diamond composite) and carbon nano tube coating, and five fin width designs (Type-a–Type-e). Five heat sinks made of aluminum material are fabricated using a wire cutting technique. The detailed dimensions of these heat sinks with base plate are presented in Table 1, respectively. The heat sink comprises a 10 x 10 array of fins and the fin pitch is constant. Both the length and width of the base of the heat sink are 80 mm. The height of the heat sink base (b) tested in the present study is 8 mm. The area of the heater is 30 x 30 mm, which is in the center of the heat sink. The heating area is heated with power of source 20 W. Multiwall carbon tubes were used as a coating material in this study. It has an average diameter of 10-20 nm and a length of 10-30 μm and was produced catalytically from hydrocarbon materials on nano catalysts under high pressure. Multiwall carbon tubes were coated on the heat sink using Physical Vapour Deposition (PVD) processor. Commercially available synthetic diamond powders of several grain sizes and copper powder (99.99% purity; -15 μm) were mixed using a powder mixer by dry process. The diamond to copper ratio of the composite material can be controlled in this mixing process. In this study the 80% volume fraction of diamond and the 20–30μm particle sizes of diamond are selected. Each mixture of diamond and copper was filled in a metal capsule and then the capsule was sealed in a vacuum under the condition of 1310 K and 6.0 x 10^{-2} Pa. The sealed capsule was pressed under the conditions of 1420–1470 K, 4.5 GPa for 15 min using a belt-type high-pressure apparatus. Its thermal conductivity is found as 448 W/m K.

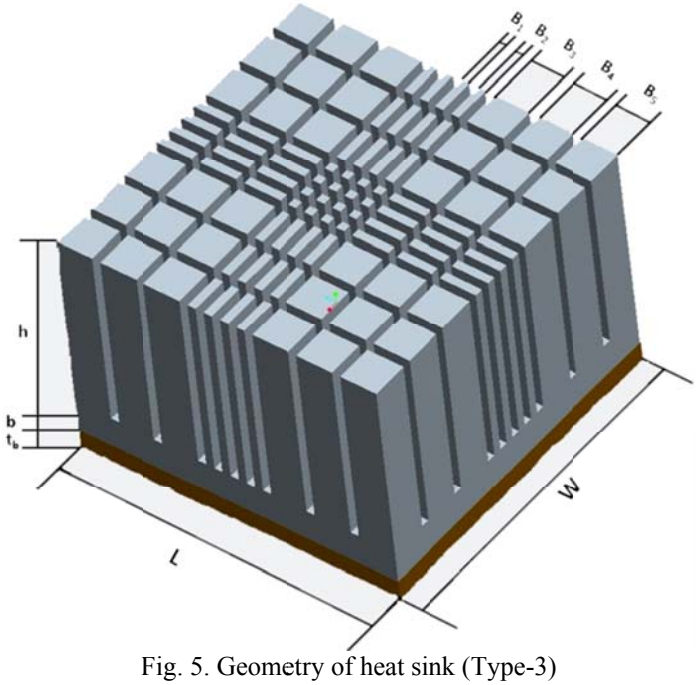

Fig. 5. Geometry of heat sink (Type-3)

Table 1. Dimensions of the fins

Fin shape	Fin Width in mm				
	B1	B2	B3	B4	B5
Type-a	2	2	9	9	9
Type-b	5	5	7	7	7
Type-c	6.2	6.2	6.2	6.2	6.2
Type-d	8	8	5	5	5
Type-e	11	11	3	3	3

L = 80 mm, W = 80 mm.

The effects of the different fin width designs on the thermal resistance of heat sink are shown in Fig. 6. It is observed from Fig. 6, the thermal resistance of heat sink decreases with increasing Reynolds number. The decrement of thermal resistance decreases gradually with the increasing Re from 15000 to 25000. As shown in Fig. 6 , the thermal performance of heat sink type b is superior to type a at Re = 5000. With increasing Reynolds number, the thermal performance of heat sink types c and d exceeds type a gradually. From this figure, except Re = 25000, we may reasonably conclude that the type e performance will exceed type a at higher Reynolds number. It is observed that the centre temperature of the heat sink is much higher than all other sides. Therefore, it is important to enlarge heat sink area and flow rate for the efficient heat dissipation in the centre region of the heat sink. In order to increase the performance of heat sink and decrease the centre temperature of heat sink, the highly thermal conductivity base plates and nano coating have been used in this paper. Although the design of type a could allow more working fluid flows into the centre of the heat sink, the fins in the centre region are too thin to dissipate heat efficiently. Therefore, the thermal resistance of type a is higher than type b.

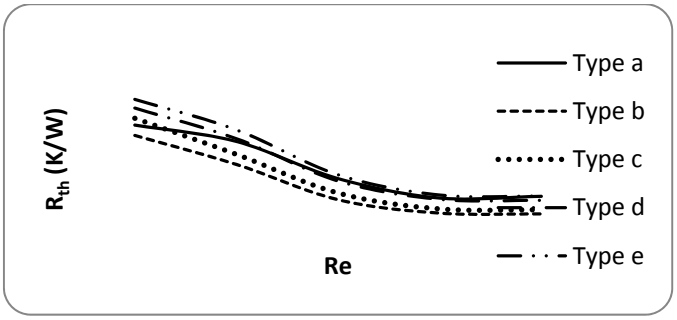

Fig. 6. Effects of the different fin width designs on thermal resistance

In Fig. 7a-e, the thermal resistance of heat sinks (Type a-e) with different base plates and nano coating are compared to those of equivalent heat sinks without base plate. In order to verify the effect of the base plates and nano coating, the other parameters of the five types of heat sink, in this case the fin width, channel width and size were equalized. As shown in Fig. 7a-e, heat sinks with CuO-Dia base plate perform better than other base plates in most experimental ranges. As shown in Fig. 7a, the heat sink with ccc base plate performance is identical with copper- diamond base plate. Heat sink with ccc base plate perform better by approximately 7.2% compared to the equivalent copper base plate heat sink in the best cases. Figure 7a shows the effects of the nano coating on thermal resistance. The thermal resistance of nano coated heat sinks are increased up to 3.3% compared to ccc base plate heat sinks. While compared to copper base plate heat sinks, the thermal performance is enhanced by approximately 5% . The trend of Fig. 7(b-e) are similar to Fig. 7a except for the heat sink with copper- diamond base plate. Its thermal performance is better than ccc base plate. The thermal resistance of type 4 and type 5 heat sink with nano coating is identical with ccc base plate at Re = 15000 to 25000.

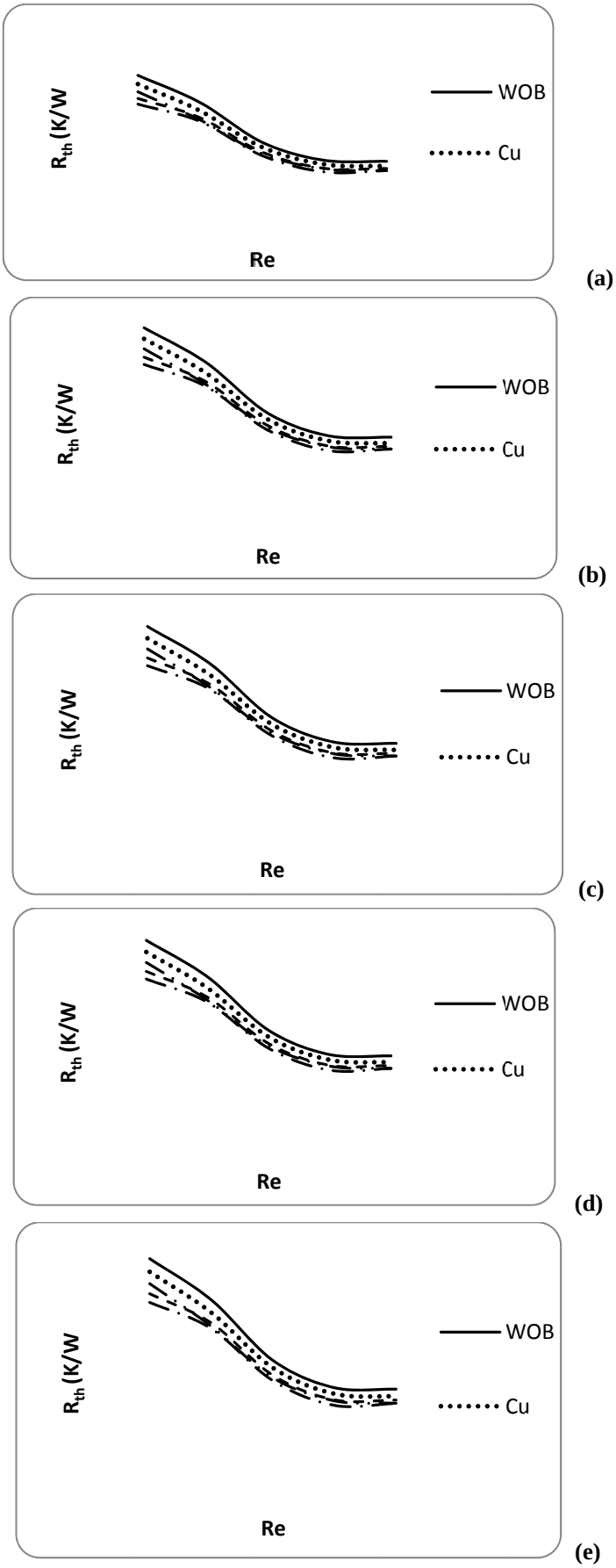

Fig. 7. Effects of the Reynolds number and different Base plates and nano coating on Thermal resistance (a) Type a (b) Type b (c) Type c (d) Type d (e) Type e

5. CONCLUSION

In this study, the effects of the base plates on thermal performance of heat sinks are experimentally investigated at various Reynolds numbers and fin dimensions. The heat transfer enhancement factors along with the thermal resistance for the heat sink with base plate and nano coating are found to be lower than the heat sink without base plate for all of the invesigated cases. This means that the use of base plates and nano coating leads to an advantage of heat transfer enhancement. In this study, it is possible to evaluate the thermal performance improvement by utilizing the un-uniform fin width design of the heat sink with base plate. It is found that an adequate un-uniform fin width design could decrease the thermal resistance. The thermal resistance of heat sink decreases with the increase of Reynolds number. It is observed that, the effects of fin dimensions on the thermal resistance at high Reynolds numbers are more obvious than that at low Reynolds numbers. The results show that there is potential to optimize the un-uniform fin width design with and without base plate.

NOMENCLATURES

b	aluminum base thickness (mm)
B	fin width (mm)
B_x , B_y , B_z	components of body force per unit volume of the fluid in x, y and z directions
ccc	carbon carbon composite
Cu	copper
Dia	diamond
f_p	fin pitch (mm)
g	gravitational acceleration (m/s^2)
h	total enthalpy (J/kg)
h	heat transfer coefficient (W/m^2K)
h	fin height (mm)
k	thermal conductivity of the fluid (W/mK)
L	heat sink Length (mm)
NC	nano coating
Nu	Nusselt number
P	pressure (bar)
Pr	Prandtl Number
Q	power generated (W)
Ra	Rayleigh Number
RANS	Reynolds averaged navier stokes
R_{th}	thermal Resistance
$T_{bm, in}$	bulk mean inlet temperature (K)
T_∞	ambient temperature (K)
t_b	base plate thickness (mm)
$T_{w,max}$	maximum wall surface temperature (K)
u, v and w	velocity components(m/s)
W	heat sink Width (mm)

Greek Symbols

ρ	density (kg/m^3)
β	coefficient of cubical expansion
Φ	viscous dissipation
$\dot{g}$	heat generation per unit volume of the fluid (W/m^3)
$\vec{V}$	velocity vector,
k_{eff}	effective thermal conductivity (W/mK)
μ_{eff}	effective viscosity
λ	second viscosity (μm)
μ	dynamic viscosity (kg/ms)

REFERENCES

1. Incropera, F. P. (1988). Convection heat transfer in electronic equipment cooling. *J. Heat transfer,* Vol. 110, pp. 1097-1111.
2. Nakayama, W. (1986). Thermal management of electronic equipment: a review of technology and research topics. *Appl. Mech. Rev*. Vol 39, No. 12, pp. 1847–1868.
3. Kim, K. S., Won, M. H., Kim, J. W. & Back, B. J. (2003) Heat pipe cooling technology for desktop PC CPU. *Appl. Therm. Eng*., Vol. 23, pp. 1137–1144.
4. Wang, Y., & Vafai, K. (2000). An experimental investigation of the thermal performance of an asymmetrical flat plate heat pipe. *Int. J. Heat Mass Transfer,* Vol. 43, pp. 2657– 2668.
5. Konda, Y., Behnia, M., Nakayama, W. & Matsushima, H. (1998). Optimization of finned heat sinks for impingement cooling of electronic packages. *J. Electronic Pack*, pp. 259-266.
6. Duan, Z., & Muzychka, Y. S. (2006). Experimental investigation of heat transfer in impingement air cooled plate fin heat sinks. *J. Electronic Pack*, Vol. 128, pp. 412–418.
7. Rahman, M. M. (2000). Measurements of heat transfer in microchannel heat sinks. *Int. Commun. Heat Mass Transf*, Vol. 27, pp. 495–506.
8. Seyf, H. R. & Layeghi, M. (2010). Numerical analysis of convective heat transfer from an elliptic pin fin heat sink with and without metal foam insert. *Journal of Heat Transfer ASME*, Vol. 132, pp. 401- 409.
9. Kim, S. Y., Koo, J. M. & Kuznetsov. (2001). Effect of anisotropy in permeability and effective thermal conductivity of an aluminum foam heat sink. *Numerical Heat Transfer, Part A: Applications*, Vol. 40, pp. 21-36.
10. Sivasankaran, H. et al. (2010). Experimental analysis of parallel plate and cross cut pin fin heat sinks for electronics cooling applications. *Journal of Thermal Science*, Vol. 14, No.1, pp. 147-156.
11. Kim, S. J., Kim, D. K. & Oh, H. H. (2008). Comparison of fluid flow and thermal characteristics of plate-fin and pin-fin heat sinks subject to a parallel flow. *Heat Transfer Engineering*, Vol. 29, issue 2, pp. 169-177.
12. Jonsson, H. & Moshfegh, B. (2001). Modeling of the thermal and hydraulic performance of plate fin, strip fin, and pin fin heat sinks-influence of flow bypass. *IEEE Transactions on Components and Packaging Technologies*, Vol. 24, pp. 142-149.
13. Kim, D. K., Jung, J. & Kim, S. J. (2010). Thermal optimization of plate-fin heat sinks with variable fin thickness. *International Journal of Heat and Mass Transfer,* Vol. 53, pp. 5988–5995.
14. Kim, T. Y. & Kim, S. J. (2009). Fluid flow and heat transfer characteristics of cross-cut heat sinks. *International Journal of Heat and Mass Transfer,* Vol. 52, pp. 5358–5370.
15. Hwang, J. J. & Lui, C.C. (1999). Detailed heat transfer characteristic comparison in straight and 90-deg turned trapezoidal ducts with pin-fin arrays. *Int. J. Heat Mass Transfer*, Vol. 42, pp. 4005–4016.
16. Hwang, J. J. & Lui, C. C. (2002). Measurement of end wall heat transfer and pressure drop in a pin-fin wedge duct. *Int. J. Heat Mass Transfer*, Vol. 42, pp. 877–889.
17. Sansoucy, E., Oosthuizen, P. H. & Ahmed, G. R. (2006). An experimental study of the enhancement of air-cooling limits for telecom/datacom heat sink applications using an impinging air jet. *J. Electron. Packaging*, Vol. 128, pp. 166–171.
18. Chiang, K. T. & Chang, F. P. (2006). Application of response surface methodology in the parametric optimization of a pin-fin type heat sink. *Int. Commun. Heat Mass Transfer*, Vol. 33, pp. 836–845.
19. Chiang, K. T., Chang, F. P. & Tsai, T. C. (2006). Optimum design parameters of pin-fin heat sink using the grey-fuzzy logic based on the orthogonal arrays. *Int. Commun. Heat Mass Transfer*, Vol. 33, pp. 744–752.
20. Li, H. Y., Chao, S. M. & Tsai, G. L. (2005). Thermal performance measurement of heat sinks with confined impinging jet by infrared thermography. *Int. J. Heat Mass Transfer*, Vol. 48, pp. 5386–5394.

21. Li, H. Y. & Chao, S. M. (2007). Thermal performance of plate-fin heat sinks under confined impinging jet conditions. *Int. J. Heat Mass Transfer*, Vol. 50, pp. 1963–1970.
22. Li, H. Y. & Chen, K. Y. (2005). Thermal-fluid characteristics of pin-fin heat sinks cooled by impinging jet. *J. Enhanc. Heat Transfer*, Vol. 12, No. 2, pp. 189–201.
23. Ozturk, E. (2007). CFD modeling of forced cooling of computer Chassis. *Engineering applications of computational fluid mechanics*, Vol. 1, pp 304-313.
24. Ozturk, E. & Tari, I. (2008). Forced air cooling of CPUs with heat sinks. *IEEE Transactions on components and packaging Technology*, Vol. 31, pp. 650-660.
25. Mohan, R. & Govindarajan, P. (2011). Experimental and CFD analysis of heat sinks with base plate for CPU cooling. *Journal of Mechanical Science and Technology, Springer*, Vol. 25, No. 8, pp. 1-10.
26. Mohan, R. & Govindarajan, P. (2011). Thermal analysis of CPU with ccc and copper base plate heat sinks using CFD. *International Journal of heat transfer – Asian research*, Vol. 40, Issue 3, pp. 217-232.
27. Yoshida, K. & Morigami, H. (2004). Thermal properties of diamond/copper composite material. *International Journal of Microelectronics Reliability*, Vol. 44, pp. 303–308.
28. Atashafrooz, M. & Gandjalikhan Nassab, S. A. (2013). Simulation of laminar mixed convection recess flow combined with radiation heat transfer. *Iranian Journal of Science & Technology, Transactions of Mechanical Engineering*, Vol. 37, No. M1, pp 71-75.